


The cold immunological landscape of ATM-deficient cancers

Sonali Sinha,¹ Victor Ng,¹ Ardijana Novaj,¹ Yingjei Zhu,² Shu Yazaki,¹ Xin Pei,¹ Fatemeh Derakhshan,³ Fresia Pareja,² Jeremy Setton,¹ Flavie Naulin,⁴ Manuel Beltrán-Visiedo,⁴ Ethan Shin,¹ Ana Leda F Longhini,⁵ Rui Gardner,⁵ Jennifer Ma,¹ Kevin Ma,¹ Anne Roulston,⁶ Stephen Morris,⁶ Maria Koehler,⁷ Simon Powell,¹ Ezra Rosen,⁸ Lorenzo Galluzzi,⁴ Jorge Reis-Filho,² Atif Khan,¹ Nadeem Riaz ¹

To cite: Sinha S, Ng V, Novaj A, *et al.* The cold immunological landscape of ATM-deficient cancers. *Journal for ImmunoTherapy of Cancer* 2025;**13**:e010548. doi:10.1136/jitc-2024-010548

► Additional supplemental material is published online only. To view, please visit the journal online (<https://doi.org/10.1136/jitc-2024-010548>).

SS and VN contributed equally.

Accepted 01 April 2025

ABSTRACT

Background Mutations in genes encoding DNA repair factors, which facilitate mismatch repair, homologous recombination, or DNA polymerase functions, are known to enhance tumor immunogenicity. Ataxia telangiectasia mutated (*ATM*) is a central regulator of DNA double-strand break repair and is frequently affected by somatic or germline mutations in various cancer types, including breast, prostate, pancreatic, and lung cancer. However, the consequences of *ATM* loss on tumor immunogenicity are poorly understood.

Methods We generated isogenic *ATM*-null models using CRISPR in murine triple-negative breast (4T1) and colorectal (CT26) cancer cell lines. *ATM* inactivation was confirmed by PCR and western blot. Immune cell infiltrates were assessed by flow cytometry and immunohistochemistry in both murine tumors and human samples from breast and lung cancers (via The Cancer Genome Atlas and institutional cohorts). In vivo, the impact of *ATM* loss on tumor growth and response to immune checkpoint blockade (anti-programmed cell death protein-1 (PD-1)) was evaluated. Furthermore, we compared the effects of different DNA-damaging agents—including an ATR inhibitor (RP-3500), a PARP inhibitor (olaparib), and the topoisomerase II inhibitor etoposide—on interferon-stimulated gene (ISG) expression and immune modulation.

Results We find that—in contrast to other DNA repair defects—*ATM* deficiency (1) fails to encourage immune effector cell infiltration into tumors, and (2) does not enable immune cell recruitment via synthetic lethality strategies in clinical trials, such as with ATR inhibition. Assessing various DNA-damaging agents in *Atm* null tumors revealed a differential activation of type I interferon (IFN) signaling, with etoposide, a topoisomerase II inhibitor, emerging as the strongest activator of ISG under these conditions. Yet, PD-1-targeted immune checkpoint blockade does not bolster the therapeutic activity of etoposide in *Atm*-null syngeneic tumor models, nor does it modify the tumor microenvironment, suggesting that type I IFN signaling alone is insufficient to overcome immunosuppression in immunologically cold *ATM* null neoplasms.

Conclusions *ATM* deficiency, while compromising DNA repair and enhancing sensitivity to radiation and ATR inhibition, does not increase tumor antigenicity or immunogenicity. Altogether, our results have important

WHAT IS ALREADY KNOWN ON THIS TOPIC

⇒ Genetic mutations in many DNA repair genes enhance tumor immunogenicity; however, whether mutations in ataxia telangiectasia mutated (*ATM*) influence tumor immunogenicity is unknown.

WHAT THIS STUDY ADDS

⇒ This study finds that *ATM*-mutated tumors have a distinct behavior from other DNA repair defective cancers, and suggests an important role for antigenicity in mediating immunogenic effects of DNA repair defects.

HOW THIS STUDY MIGHT AFFECT RESEARCH, PRACTICE OR POLICY

⇒ Novel approaches are necessary to enhance the immunogenicity of *ATM*-mutated cancers.

implications for the design of novel combination therapies for *ATM* null tumors and highlight the importance of antigenicity in the immunological consequences of defective DNA repair.

INTRODUCTION

The DNA damage response (DDR) encompasses a complex network of proteins, which can be broadly organized into three categories: (1) sensors of DNA damage, (2) proteins that integrate the DDR with other cellular activities (eg, the cell cycle), and (3) effector proteins that repair specific DNA lesions.^{1 2} Deficiency in the DDR is an enabling hallmark of cancer and manifests across many cancer types.^{3 4} The most common DDR deficiencies in cancer include aberrations in specific repair pathways, including mismatch repair (MMR), homologous recombination (HR), nucleotide excision repair, and DNA synthesis by polymerases (eg, polymerase epsilon, POLE). These deficiencies are often caused by either hereditary mutations in the germline or somatic mutations



© Author(s) (or their employer(s)) 2025. Re-use permitted under CC BY-NC. No commercial re-use. See rights and permissions. Published by BMJ Group.

For numbered affiliations see end of article.

Correspondence to

Dr Nadeem Riaz;
riazn@mskcc.org

Atif Khan; khana7@mskcc.org

that accumulate during oncogenesis, both of which are thought to enable acquisition of other alterations to facilitate disease progression.

Intriguingly, specific DDR deficiencies such as those found in mismatch repair deficiency (MMRd), homologous recombination deficiency (HRD), and POLE alterations are well known to promote cancer immunogenicity and increase immune cell infiltration.^{5–7} MMR and POLE deficient cancers exhibit a substantial mutational burden (10–100-fold higher than histologically matched control tumors), leading to an increase in neoantigen burden, a factor believed to drive their heightened immunogenicity.⁸ Tumors with MMRd are indeed so immunogenic that the Food and Drug Administration approved immune checkpoint blockade with anti-programmed cell death protein-1 (PD-1) agents in the metastatic setting regardless of histology and anti-PD-1 is further being considered for curative treatment in lieu of surgery in this context.⁹ In contrast, HRD tumors exhibit a modest increase in mutational burden (twofold higher than their HR-proficient counterparts), but they have a brisk immune infiltrate and distinct responses to anti-PD-1 therapy.¹⁰ Interestingly, HRD tumors may also stimulate immune responses by activating intracellular sensors of cytosolic nucleic acids,^{11,12} resulting in the abundant secretion of pro-inflammatory cytokines including type I interferon (IFN).¹³

After MMR and HR, genetic alterations in ataxia telangiectasia mutated (*ATM*) are the third most common DDR defect in cancer, with somatic and/or germline mutations occurring in 1–5% of all cancers.¹⁴ *ATM* belongs to the PIKK superfamily and is a central regulator of the cellular response to DNA double-strand breaks.¹⁵ Homozygous loss of *ATM* in the germline causes a rare inherited autosomal recessive disorder known as ataxia telangiectasia, which is characterized by a syndrome of immunodeficiency, cerebellar ataxia, radiation sensitivity, and increased risk of cancer.^{16,17} Similar to MMR and HR, heterozygous loss of *ATM* in the germline is associated with increased cancer risk,¹⁸ and somatic alterations occur during oncogenesis in a number of cancer types.^{14,19}

Here, we sought to elucidate the impact of *ATM* alterations on tumor-targeting immunity using patient samples and isogenic mouse models of breast and colorectal cancer. We found that, unlike cancers with other DDR defects, *ATM* null mouse and human tumors are not immunogenic and that synthetic lethality strategies currently tested in the clinic, notably ataxia telangiectasia and rad3-related protein (ATR) inhibitors, do not facilitate immunity for *ATM* null cancers. Finally, we demonstrate that abundant type I IFN secretion, as driven by the topoisomerase II inhibitor etoposide in these tumors, is insufficient to restore immune infiltration and sensitivity to PD-1 blockers. Altogether, our findings indicate that *ATM*-deficient tumors have a distinct immunological profile from other DDR-defective tumors and emphasize the critical role of antigenicity in the immune sequelae of compromised DNA repair.

RESULTS

ATM null cancer models are sensitive to radiation but not immunogenic and do not respond to immune checkpoint blockade

We assessed the impact of *ATM* deficiency on tumor immunogenicity using the GenCRISPR system (GenScript) to create isogenic mouse models of triple-negative breast cancer (4T1 cells) and colorectal cancer (CT26 cells), as we have previously done.^{10,20,21} PCR identified insertion/deletion events in *Atm* leading to truncation, and western blot confirmed knockout of *Atm* (online supplemental figure 1A–C). Importantly, in knockout models, ATM signaling post-ionizing radiation was abolished, as evidenced by a marked reduction in the phosphorylation of canonical ATM target KAP1, compared with wild-type controls (figure 1A).²² As anticipated, *Atm* null models were more sensitive to radiation as indicated by decreased cell viability compared with isogenic controls (figure 1B). Lastly, we observed elevated nuclear γ -H2AX foci, indicating persistent DNA damage, in *Atm* null cells 24 hours after recovery from exposure to 10 Gy of radiation (figure 1C). Altogether, these results indicate that our *Atm* null 4T1 and CT26 tumor models recapitulate classical DNA repair defects of *ATM*-deficient tumors.

We next sought to evaluate the impact of *Atm* deficiency on the immune landscape of tumors using these models. In contrast to other DNA repair defects,^{10,20,21} flow cytometry of both 4T1 and CT26 tumors did not reveal any difference in bulk CD3⁺ T cells, bulk CD8⁺ T cells or their activated (GZMB⁺) or proliferating (KI67⁺) subsets compared with isogenic controls (figure 1D, online supplemental figure 1D). Consistent with this finding, immunohistochemistry (IHC)-based on the pan-T cell marker CD3 (figure 1E) also did not illustrate an increase in T-cell infiltration. We subsequently sought to evaluate whether *Atm* null tumors may still be responsive to immune checkpoint blockade (ICB). However, in both 4T1 and CT26 models, anti-PD-1 therapy was not more effective in *Atm* null tumors than in their isogenic controls (figure 1F, online supplemental figure 1E). Not surprisingly, *Atm* null tumors grew slower than wild-type (WT) models, consistent with prior findings showing reduced proliferation.^{23–26} In summary, while our *Atm* null models replicate classic DNA repair deficiencies, they suggest that loss of *Atm* does not change the immunological tumor microenvironment (TME) or increase sensitivity to ICB.

ATM loss does not increase T-cell infiltration in human cancer

We subsequently aimed to assess the impact of *ATM* deficiency on the immunological TME of breast and lung cancer in humans. We first explored the influence of pathogenic mutations in *ATM* in breast cancer by examining immune de-convolution data from TCGA as well as IHC data from patients at our institution. In contrast to patients with other DNA repair defects,^{6,10,27} patients with breast cancer harboring pathogenic *ATM* mutations showed no difference in intratumoral T-cell abundance compared with patients with wild-type tumors (figure 2A).

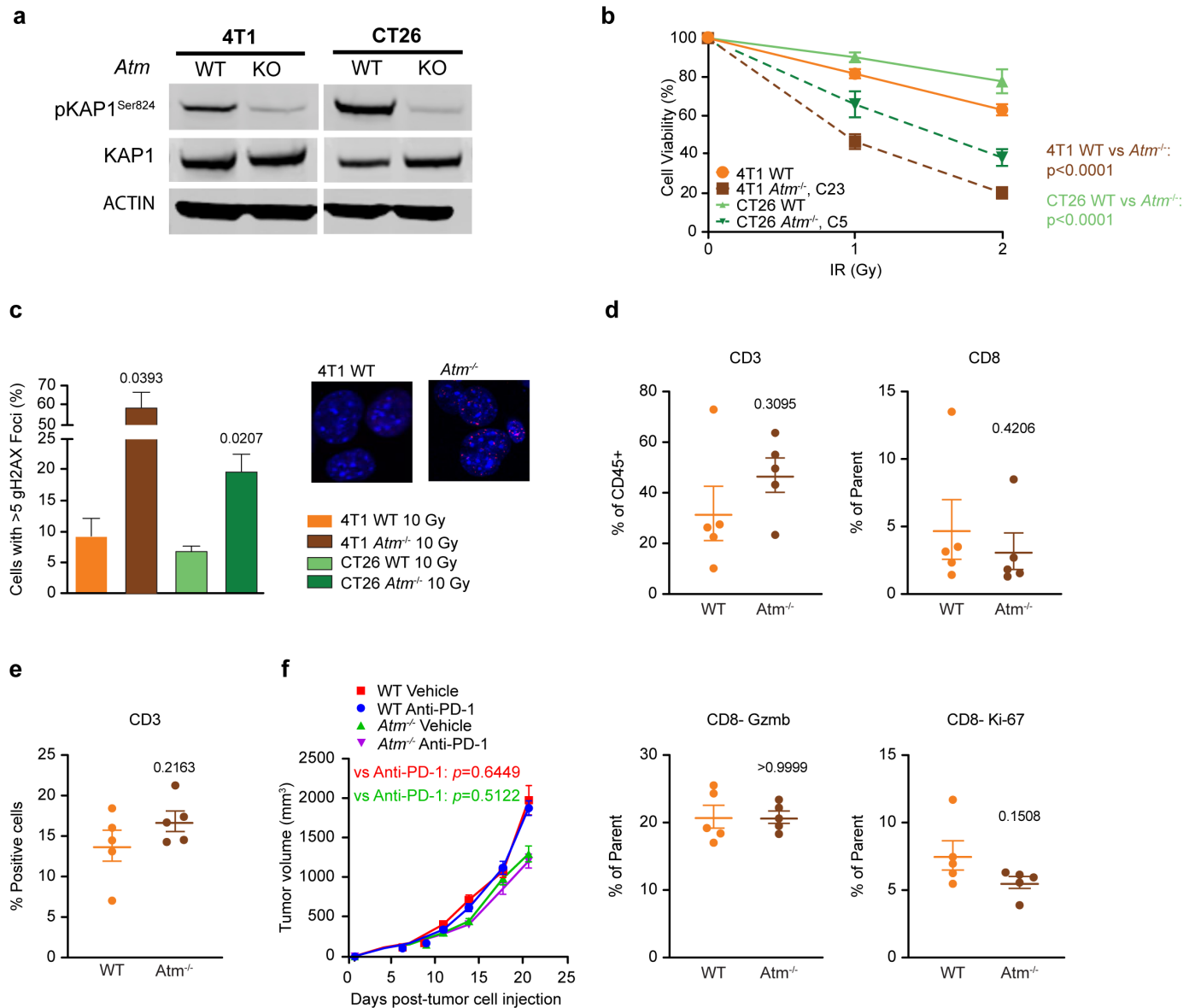


Figure 1 *Atm*^{-/-} models recapitulate canonical features of *Atm* deficiency and are non-immunogenic. (A) After 10Gy IR, the *Atm*^{-/-} 4T1 (Clone T3-23) or CT26 (Clone 5) cells do not demonstrate phospho-Kap1 (Serine 824) signaling compared with wild-type controls. (B) In vitro cellular viability identifies *Atm*^{-/-} 4T1 and CT26 models as significantly more sensitive to IR than parental controls (n=3 biologic replicates, mean±SD, ordinary two-way analysis of variance). (C) Results of γ-H2AX immunofluorescence analysis performed in 4T1 cells 24 hours after irradiation. Cell nuclei with >15 foci were scored as positive. Inset showing representative images of γ-H2AX immunofluorescence (green). Nuclei were counterstained with 6-diamino-2-phenylindole (blue). (D) In vivo assessment of immune infiltrate in 4T1 models by flow cytometry demonstrates similar T-cell populations as the WT from tumors sacrificed at 16 days (n=5 tumors per group; data represented as mean±SEM, two-tailed unpaired Student's t-test). (E) In vivo assessment of immune infiltrate by immunohistochemistry from 4T1 models (n=5 mice per group, data represented as mean±SD; two-tailed unpaired Student's t-test). (F) Parental 4T1 and *Atm*^{-/-} tumors show no response to anti-PD-1 suggesting lack of immunogenicity in a 4T1 model. ATM, ataxia telangiectasia mutated; KO, knock out; IR, ionizing radiation; PD-1, programmed cell death protein-1; WT, wild-type.

Similarly, the IHC-based analysis of *ATM*-mutated patients with estrogen receptor-positive breast cancer, matched by age and grade to controls (online supplemental figure 2A), revealed no increase in CD4+, CD8+, or total T-cell counts within the stroma or tumor (figure 2B,C). To determine if cancer histology could explain this effect, we evaluated T-cell infiltrate in patients with lung cancer from the TCGA, as lung cancer has a high frequency of pathogenic mutations in *ATM*. Similar to breast cancer,

ATM-mutated lung cancers did not have an increase in T-cell infiltrate compared with wild-type tumors either (figure 2D). Similarly, colorectal cancers also illustrated that *ATM* mutated tumors did not have an increase in CD8 T cells, whereas those that were MSI or POLE altered did (online supplemental figure 2B). Furthermore, measurements of tumor mutation burden illustrated comparable levels between *ATM* mutated and wild-type breast or lung cancer tumors in patients (figure 2E). Altogether, these

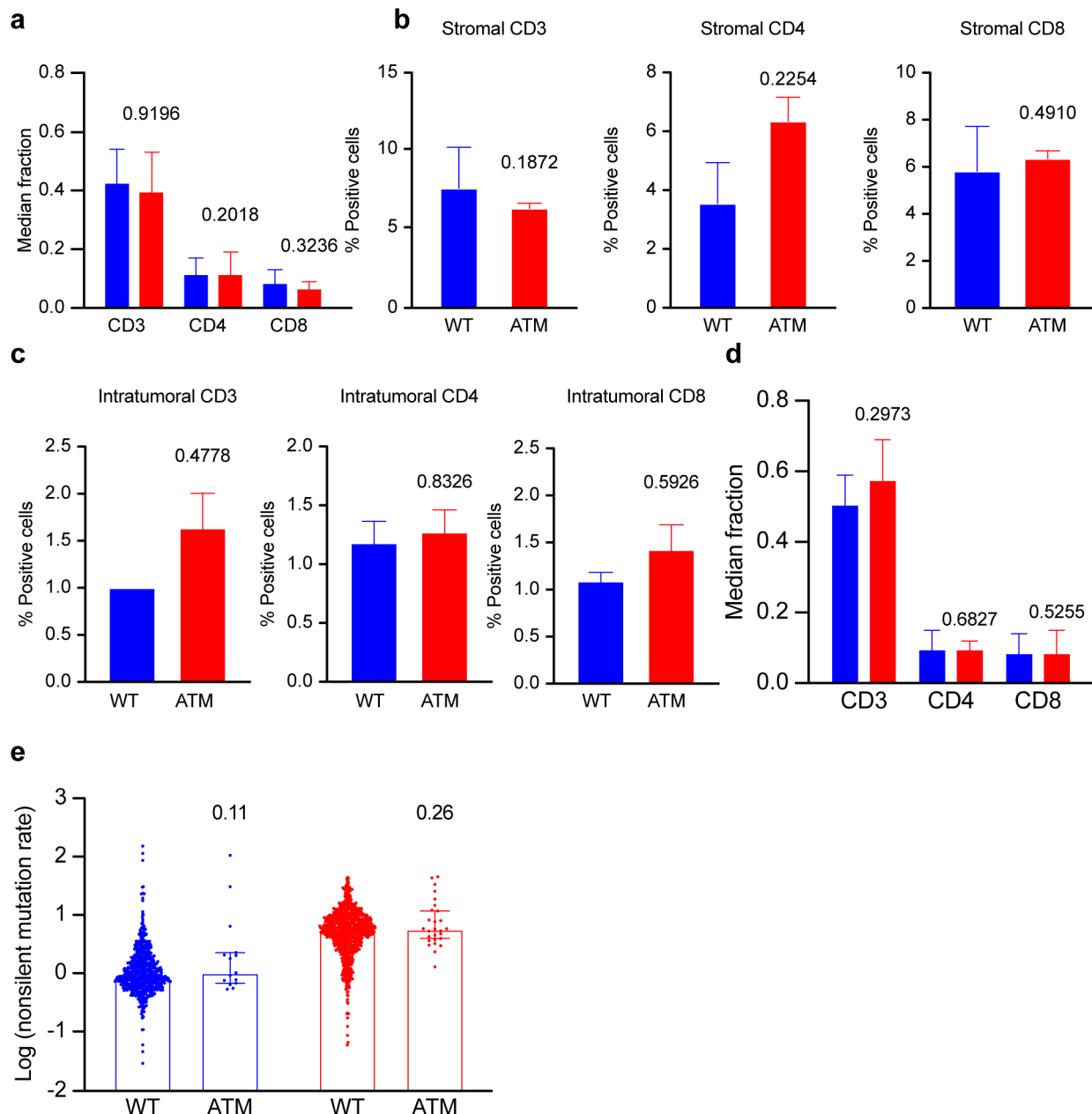


Figure 2 *ATM* mutations do not increase T-cell infiltration in human tumors. (A) TCGA analysis of *Atm*^{-/-} tumors in patients with breast cancer (data are represented as mean±SD, Mann-Whitney U test). (B) Immunohistochemistry of T-cell markers CD3, CD4 and CD8 does not show any difference in infiltration in the stromal environment in tumors of the patients with breast cancer (mean±SD, two-tailed unpaired Student's t-test). (C) Intratumoral T-cell infiltration was not found in the patients with breast cancer. (Mean±SD, two-tailed unpaired Student's t-test). (D) TCGA analysis of *Atm*^{-/-} tumors in patients with lung cancer (data are represented as mean±SD, Mann-Whitney U test). (E) Tumor mutation burden of *ATM* mutated tumors in patients with breast or lung cancer (data are represented as mean±SD, Mann-Whitney U test). *ATM*, ataxia telangiectasia mutated; TCGA, the cancer genome atlas; WT, wild-type.

data are consistent with our findings in syngeneic murine models and suggest that pathogenic *ATM* mutations do not markedly alter the immune TME of human breast and lung cancer.

Targeted therapy with ATR inhibition does not modulate the immunological TME in *Atm* null tumors

Some therapies targeting DNA repair partly function by eliciting an immunological response. For instance, poly ADP-ribose polymerase (PARP) inhibitors in HRD

cancers have been shown to involve a reconfiguration of the immunological TME coupled with the activation of immune effector mechanisms.^{28 29} Hence, we posited that DNA repair-directed therapeutics currently being investigated in the clinic for *ATM* null tumors may also modulate the TME. ATR inhibitors are synthetically lethal in *ATM* null tumors, with several distinct compounds in early phase clinical trials.³⁰ We tested a best-in-class ATR inhibitor, RP-3500 (camonsertib)

and, as anticipated, identified a preferential decrease in cell viability in *Atm*^{-/-} 4T1 cells over their wild-type counterparts (figure 3A). We next evaluated the effect of ATR inhibition in vivo by implanting 4T1 cells orthotopically in the mammary fat pad of syngeneic BALB/c mice and treating them with RP-3500 (15–30 mg/kg of body weight) or vehicle. In line with in vitro findings, we documented a significant dose response with a 60% remission rate at the previously established MTD for RP-3500 (figure 3B). In contrast, parental (*Atm* competent) 4T1 tumors developing in immunocompetent syngeneic hosts were not sensitive to ATR inhibition (online supplemental figure 3A).

Although there was significant growth delay in *Atm* null tumors receiving RP-3500, IHC revealed no increase in intratumoral T cells relative to vehicle-treated *Atm*-deficient tumors (figure 3C; online supplemental figure 3B). Similarly, flow cytometry of dissociated tumor cells did not reveal a change in T-cell frequency but identified a significant decrease in the activation and proliferation of the intratumoral CD8 T cells post RP-3500 treatment as compared with vehicle (figure 3D). These findings align with recent work demonstrating that ATR inhibitors selectively impair CD8 T-cell proliferation³¹ likely due to their more rapid proliferative kinetics following cytotoxic therapies.³²

To further evaluate the role of the immune system in response to ATR inhibition in ATM null models, we assessed efficacy in immunodeficient NSG mice and immune-competent mice with CD8 T cells depleted. We first injected NSG mice with the 4T1 *Atm* null cells and found that RP-3500 showed similar efficacy in the absence of the immune cells (figure 3E). To further assess the role of CD8 T cells in the efficacy of RP-3500, we compared the treatment of RP-3500 with and without depletion of CD8⁺ T cells in Balb/c mice injected with 4T1 *Atm* null cells. As anticipated, treatment with anti-CD8 Ab led to a specific decrease in the CD8⁺ T-cell subset when compared with the IgG treated group (online supplemental figure 3C). Yet, the efficacy of RP-3500 was similar with or without CD8 T-cell depletion (figure 3F). Together, these results indicate that inhibition of tumor growth by RP-3500 is independent of the T cells in this genotype.

Despite the lack of overt signs of immunogenicity, we decided to evaluate whether ATR inhibition could still be synergistic with ICB with a PD-1-targeting agent. Unfortunately, the addition of a PD-1 blocker failed to improve the efficacy of RP-3500 against *Atm*^{-/-} 4T1 lesions growing orthotopically in immunocompetent syngeneic mice (figure 3G). Similar results were obtained with an alternative *Atm*^{-/-} 4T1 single cell clone (online supplemental figure 3D). Flow cytometric analysis showed that co-administration of an anti-PD-1 antibody did not restore the diminished activity and proliferation of CD8⁺T cells induced by RP-3500 in the TME of *Atm*-deficient 4T1 tumors (figure 3H). That said, therapy was well tolerated with a maximum of 10% drop in body weight post-treatment (data not shown).

We subsequently sought to evaluate the impact of ATR inhibition on the TME of patients with cancer treated with RP-3500 in the context of a phase 1 clinical trial (NCT04497116), profiling the TME both before treatment and 5–6 weeks after treatment initiation (figure 4A). Focusing on patients with pathogenic *ATM* mutations, we failed to observe significant changes in T-cell infiltration during therapy (figure 4B). Similarly, the cytolytic score (a transcriptional signature of T-cell activation) did not significantly increase during therapy (figure 4C), nor did intratumoral macrophages (figure 4D). Altogether, these data suggest that the loss of *ATM* markedly increases the sensitivity of cancer cells to ATR inhibition via non-immunological mechanisms that cannot be significantly potentiated with ICB.

DNA-damaging agents differ in their ability to elicit IFN signaling in *Atm* null tumors

As ATR inhibition failed to modulate the immunological TME of *Atm* null tumors, we sought to understand how ATR inhibition and other DNA damaging therapeutics modulated immune activation by focusing on the expression of canonical interferon-stimulated genes (ISGs) such as C-X-C motif chemokine ligand 10 (*Cxcl10*), IFN beta 1 (*Ifnb*) and IFN-induced 15 kDa protein (*Isg15*). Alongside RP-3500, we assessed ISG responses to a topoisomerase II inhibitor, etoposide, and a PARP inhibitor, olaparib. Etoposide is known to produce double-stranded DNA breaks and is active against *Atm* null tumors. We observed robust induction of ISG expression in *Atm*^{-/-} 4T1 cells exposed to etoposide for 24 hours (figure 5A). Conversely, olaparib resembled RP-3500 in its inability to elicit the expression of ISGs in this genotype (figure 5A). Incubations from 2 to 48 hours also did not result in increased ISG expression following RP-3500 treatment (online supplemental figure 4A–E). Importantly, differences in ISG responses between treatments were not due to differences in cell viability, as 24 hours post-treatment viability was comparable for all agents (60–70%, online supplemental figure 4F). In contrast, combination treatment with RP-3500 and olaparib resulted in significant ISG upregulation in *Atm*-null 4T1 cells (figure 5B), although less pronounced than with etoposide (figure 5A).

Together, these results indicate that IFN signaling in *Atm* null cells depends on the precise type of DNA damage and cell death elicited by the initiating stimulus, with a strong dependence on the class of agent.

IFN signaling is not sufficient to alter the TME in poorly immunogenic *Atm* null tumors

Finally, we evaluated the effect of IFN signaling as elicited by etoposide in cultured *Atm*^{-/-} 4T1 cells on immunological parameters in vivo. As anticipated, both wild-type and *Atm* null 4T1 lesions established orthotopically in immunocompetent syngeneic hosts responded to etoposide, with the latter exhibiting superior sensitivity (figure 6A,B). Surprisingly though, the addition of a PD-1 blocker failed to improve the therapeutic activity of etoposide in *Atm*

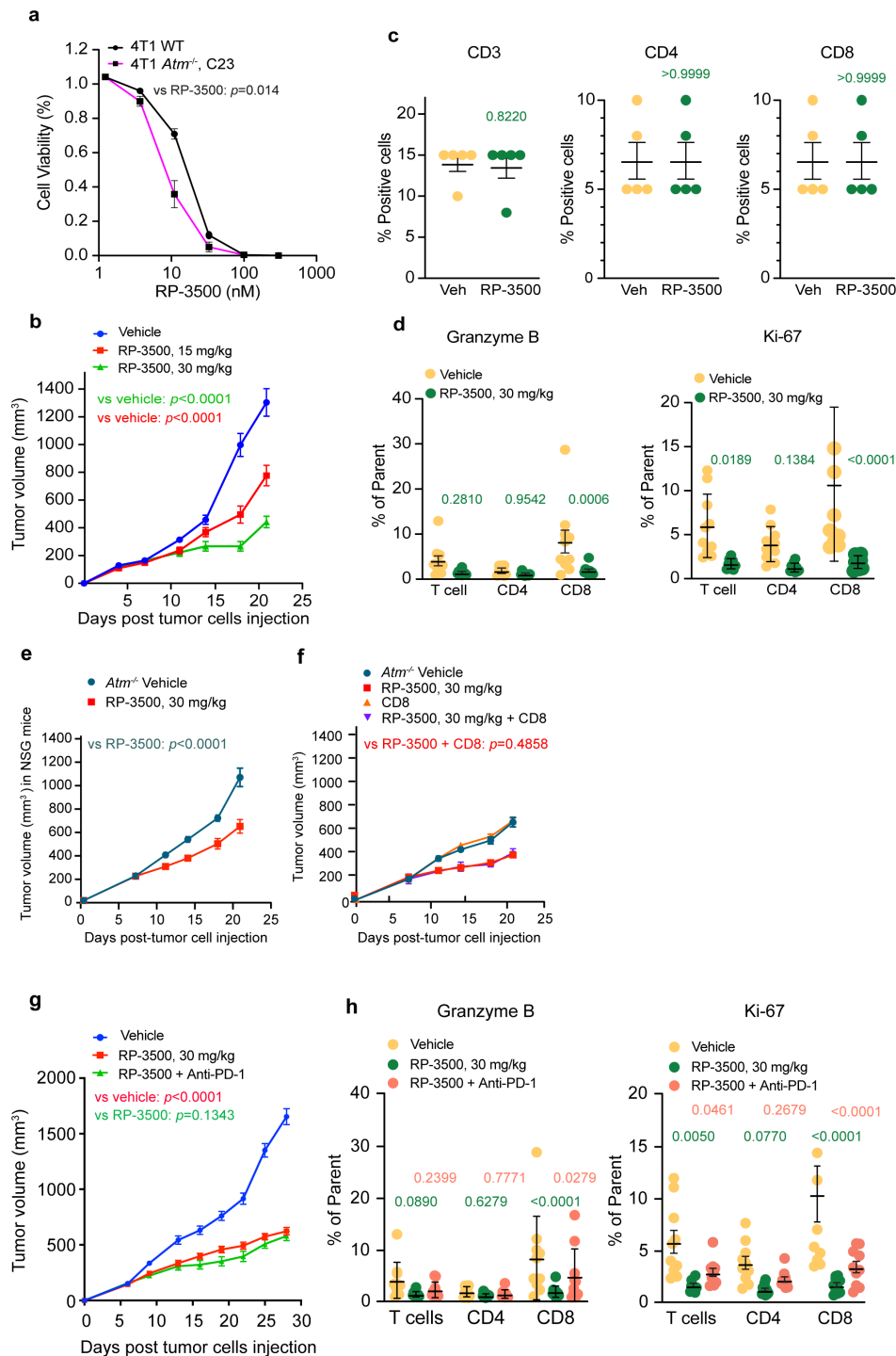


Figure 3 ATR inhibition in *Atm*^{-/-} tumors is non-immunogenic. (A) *Atm*^{-/-} 4T1 cells are sensitive to RP-3500 in vitro with an IC₅₀ of 8.6 nM (n=3 biologic replicates). (B) In vivo growth inhibition identifies a dose-response effect between RP-3500 and growth delay in *Atm*^{-/-} tumors (data from three independent replicates, data are represented as mean±SEM, two-way ANOVA, Sidak's multiple comparisons test). (C) Immunohistochemistry of treated tumors at day 16 identifies no significant increase of T cells (n=5 tumors per group; mean±SD, two-tailed unpaired Student's t-test). (D) Flow cytometry--based immunophenotyping identifies depletion of proliferation and activation in CD8 T cells (n=10 mice per group; data are represented as mean±SEM; two-tailed unpaired Student's t-test). (E) 4T1 *Atm*^{-/-} tumors show significant response to RP-3500 in the immunodeficient NSG mice. (F) Efficacy of RP-3500 does not alter post CD8+T cells. Results are expressed as the mean value of three independent experiments. (n=10 mice per group, data are represented as mean±SEM, two-way ANOVA, Sidak's multiple comparisons test). (G) Combination therapy with RP-3500 and anti-PD-1 does not lead to further growth delay (n=10 mice per group, data are represented as mean±SEM, two-way ANOVA, Sidak's multiple comparisons test). (H) Immunophenotyping by flow cytometry shows a decrease in proliferation and cytotoxic activity of CD8 T cells (n=10 mice per group, data are represented as mean±SEM, two-way ANOVA). ATR, ataxia telangiectasia and rad3-related protein; ANOVA, analysis of variance; ATM, ataxia telangiectasia mutated; PD-1, programmed cell death protein-1.

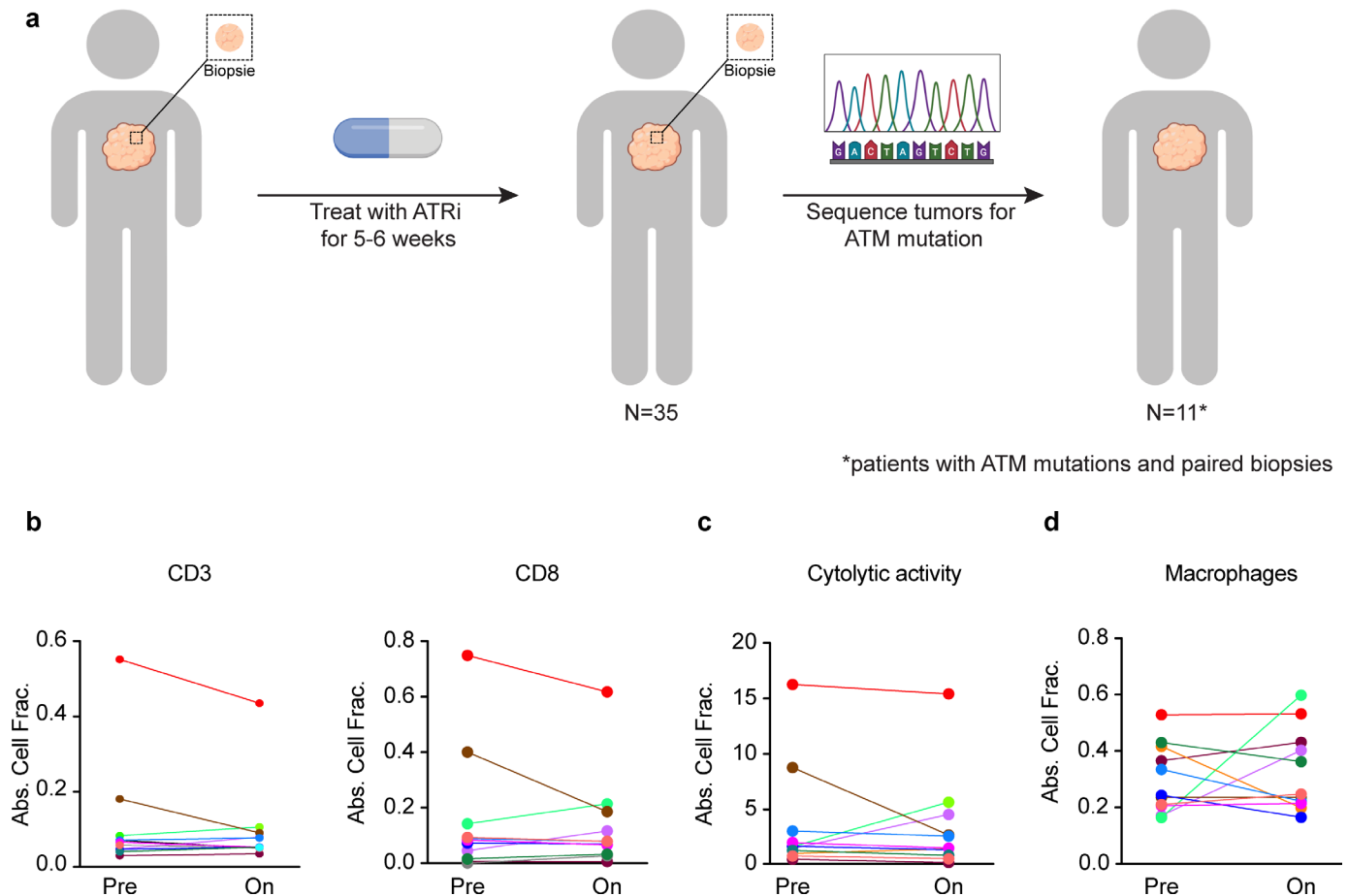


Figure 4 Immunologic activity of ATR inhibition in human patients. (A) Clinical trial schematic of RP-3500 monotherapy. (B) Immune deconvolution results of pre-therapy and post-therapy biopsies identify no significant increase in overall T cells or CD8 T cells (data are represented as mean±SEM; two-tailed unpaired Student's t-test). (C) Evaluation of T-cell activation does not identify a significant increase in cytolytic score with ATR inhibition (data are represented as mean±SEM; two-tailed unpaired Student's t-test). (D) Macrophage cell infiltration does not increase in the tumors with ATR inhibition (data are represented as mean±SEM; two-tailed unpaired Student's t-test). ATM, ataxia telangiectasia mutated; ATR, ataxia telangiectasia and rad3-related protein.

null 4T1 and CT26 tumors (figure 6B,C). In line with this notion, etoposide failed to alter the immunological TME of *Atm* null 4T1 tumors growing in the mammary fat pad of BALB/c mice, a defect that could not be reverted with PD-1 blockade (figure 6D), despite (at least partial) signs of ongoing type I IFN signaling 3 and 7 days after treatment initiation (figure 6E). These data suggest that DNA repair-directed therapies that increase IFN signaling may not be sufficient to enable ICB activity in poorly immunogenic tumors.

DISCUSSION

Here, we used syngeneic mouse models of breast and colorectal cancer and data from patients with breast and lung carcinoma to elucidate the impact of *ATM*, a commonly inactivated tumor suppressor, on anticancer immunity. In both model systems and human cancers, we failed to observe signs of immune activation or superior ICB sensitivity as a consequence of *ATM* loss. We evaluated several different classes of therapeutics currently

investigated for *ATM* null tumors, including ATR inhibitors, PARP inhibitors, and cytotoxic chemotherapy, finding class-dependent activation of IFN signaling that—however—was insufficient to restore ICB activity in our models.

Surprisingly, unlike other common DNA repair defects in cancer such as deficiencies in HR, MMR and POLE, which are known to increase cancer cell antigenicity and drive IFN signaling downstream of the accumulation of nucleic acid in the cytosol,^{6 7 33} *ATM* loss failed to drive anticancer immune responses. Hereditary defects in *ATM* have been previously shown to activate nucleic acid sensors and lead to chronic inflammation.³⁴ However, our data, as well as data from others, suggest that the loss of *ATM* does not substantially increase tumor mutational burden.³⁵ Further, in both human tumors and our isogenic models, we did not observe evidence of increased T-cell infiltrate on *ATM* loss. These results suggest that although innate IFN signaling is likely to be important for anticancer immunity,^{36 37} it may not be sufficient by itself

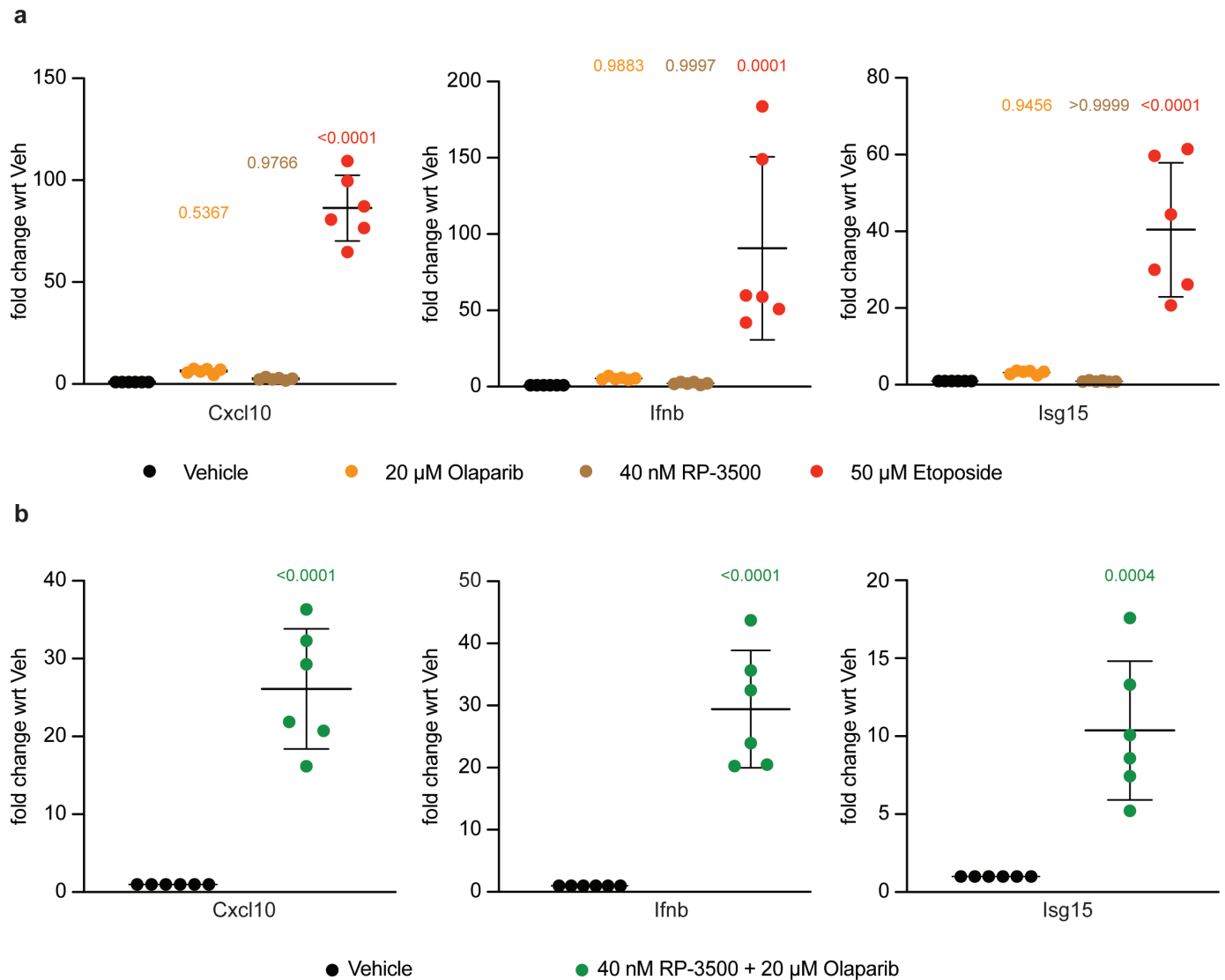


Figure 5 *Atm*-targeted therapeutics have distinct interferon activation profiles. (A) Induction of interferon-stimulated genes in 4T1 cells treated with RP-3500, olaparib or etoposide (data are represented as mean \pm SD, two-way ANOVA, Dunnett's multiple comparisons test). (B) Increased induction of interferon response with combination treatment of RP-3500 and olaparib in *Atm*^{-/-} cells. (Data are represented as mean \pm SD, two-way ANOVA, Dunnett's multiple comparisons test). ANOVA, analysis of variance; ATM, ataxia telangiectasia mutated.

to explain the immunogenicity of DDR-defective tumors, and likely a combination of both antigenicity and innate signaling is required.

Interestingly, we observed marked differences between different DNA repair-directed therapies on activation of IFN signaling. Although both ATR inhibition and etoposide similarly decreased cellular viability *in vitro*, they had markedly different effects on ISG induction, highlighting the importance of mechanisms of cell death on activation of immunologic signaling.^{38–40} Etoposide produces significant DNA damage and cytosolic DNA accumulation whereas synthetic lethality from ATR inhibition in *Atm* null cells is thought to emerge, at least in part, from abrogation of cell cycle checkpoints. Prior work has shown that ATR inhibition may potentiate anticancer immunity if combined with other DNA-damaging agents.⁴¹ Concordant with this, we also observed a significant increase

in ISGs when combining ATR and PARP inhibitors. However, despite some of the DNA repair-directed therapies that we tested robustly activating IFN signaling, none synergized with ICB *in vivo*. These data suggest that novel approaches are needed to activate the immune system against *ATM* null tumors.

Apparently at odds with our results, mouse pancreatic cancer mT4 and KPC2 cells subjected to ATM depletion with shRNA and established subcutaneously in immunocompetent syngeneic hosts exhibited improved responses to PD-1 therapy combined with radiotherapy.⁴² This may reflect lineage-specific effects (pancreas vs breast and colon), marked differences in growth kinetics (faster growth in the models used here), or the method employed for *ATM* depletion (with a potential immunogenicity for shRNA constructs).⁴³ Our results are also in contrast with previous work harnessing 4T1 cells and CRISPR/Cas9 as

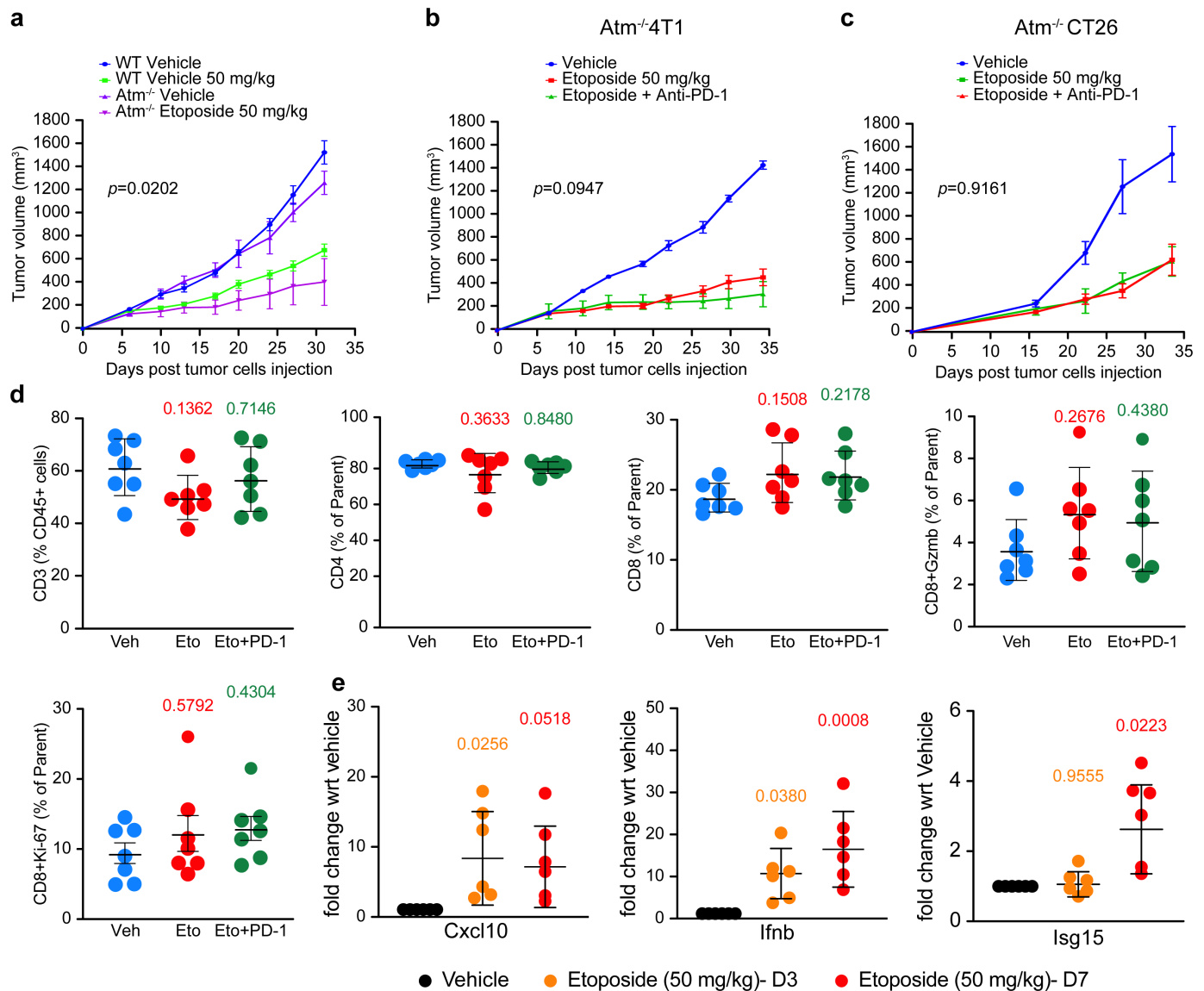


Figure 6 Activation of interferon signaling is not sufficient to synergize with anti-PD-1. (A) Tumor growth curve exhibits significant delayed growth in the *Atm*^{-/-} in comparison to the parental tumors with the etoposide drug treatment (n=8 mice per group; data represented as mean±SEM, two-way ANOVA). (B) The treated mice did not benefit from the addition of anti-PD-1 with the etoposide in the 4T1 model (n=8 mice per group; data represented as mean±SEM, two-way ANOVA). (C) Etoposide combination with anti-PD-1 did not increase the treatment efficacy of the etoposide monotherapy in the CT26 model similar to the 4T1 model (n=8 mice per group; data represented as mean±SEM, two-way ANOVA). (D) Immuno-phenotyping by flow cytometry shows no significant alterations in the T-cell population or proliferation and activation with etoposide or combination treatment in the *Atm*^{-/-} 4T1 mouse tumors (n=7 mice per group; data represented as mean±SEM, ordinary one-way ANOVA with Tukey's multiple comparisons test). (E) Significant increase in the induction of interferon response genes was detected with etoposide or combination therapy in *Atm*^{-/-} mouse tumors (data are represented as median, two-way ANOVA, Dunnett's multiple comparisons test). ANOVA, analysis of variance; ATM, ataxia telangiectasia mutated; Cxcl10, C-X-C motif chemokine ligand 10; Ifnb, interferon beta 1; ISG, interferon stimulated gene; PD-1, programmed cell death 1.

a strategy for *Atm* inactivation, which ultimately resulted in robust immunogenicity coupled with tumor rejection shortly after implantation.⁴⁴ We hypothesize that these differences may be due to persistent expression of Cas9, which has been shown to be highly immunogenic.⁴⁵

Despite these and other unsolved questions, here we demonstrate that unlike cancers with other defects in DNA repair, *ATM* null tumors are not immunogenic, both in mice and humans. Moreover, we show that clinically used DNA repair-directed therapies differ in their capacity to elicit IFN

signaling in *Atm* null tumors, and that even those with superior ISG activity (such as etoposide) may be insufficient to convert immunologically cold *ATM* null lesions into hot tumors that respond to ICB. In conclusion, our data suggest that unique strategies will be necessary to activate the immune system in patients with *ATM*-null tumors.

METHODS

Test compounds

RP-3500 (Repare Therapeutics) was prepared as described in Roulston *et al*, 2022, olaparib and etoposide (MedChem Express, #HY-10162, #HY-13629) were purchased.⁴⁶

Generation of mouse isogenic cell lines

4T1 and CT26 cell lines were purchased from American Type Culture Collection (ATCC) before manipulation. CRISPR knockout cell lines were developed by using GenCRISPR gene editing technology (GenScript). Based on the genomic sequence of *Atm*, target sites were located according to the rules of designing a targeting guidance RNA for the GenCRISPR system. By transient transfection of RNP (GenScript CRISPR single-guide RNAs: Cas9), the endogenous target gene was targeted and mutated, resulting in consequential reduction (or removal) of the expression of the encoded protein. Isogenic knockout cell clones were generated by cultivating diluted transfected cells in 96-well plates and were identified by Sanger sequencing screening. For the 4T1 cell line, we have used two full-allelic knockouts Clone T3-23 and Clone T3-29. For the CT26 line, two full-allelic knockouts Clone 5 and Clone 35 was used. Cells were cultured in Roswell Park Memorial Institute (RPMI) 1640 media with 10% fetal bovine serum (FBS) and were used at passages of less than 20 from the initial source vial.

Cellular viability assays

4T1 or CT26 cells were seeded in triplicates in opaque 96-well plates at a concentration of 200 cells per well in a 96-well plate and subsequently irradiated at a dose of 1 or 2 Gy. Control non-irradiated plate of cells was also included in the experiments. Cell viability was assessed 4–5 days after seeding, using a luminescent cell viability assay (CellTiter-Glo, Promega). 4T1 cells were treated with different concentrations of RP-3500 to measure cell viability and IC₅₀ by CellTiter-Glo assay post 4–5 days. 4T1 *Atm* knock out (KO) cells were treated with different doses of olaparib, etoposide or RP-3500 to assess the viability of cells post 24 hours treatment. Cell viability assessed for each experiment was repeated at least three times.

Human TCGA analysis

We downloaded immunogenomic data from previous pan-cancer analysis of the TCGA data set.⁴⁷ We extracted ATM and BRCA1/2 mutation profiles from our previous work.⁴⁸ Cases with both immunogenomic data and mutation profiles were used in the further analysis. Given that the frequency of ATM and BRCA1/2 mutations varies by cancer type, we used data from breast cancer, lung adenocarcinoma and lung squamous cell carcinoma as TCGA cancer types for analysis. We compared immune cell fractions and non-silent mutation rates in tumors with ATM pathogenic mutation and wild type. Tumors with BRCA1/2 mutations were excluded from the analysis. Immune cell fractions were estimated using CIBERSORT.⁴⁹ Cell types of lymphocytes and CD4 T cells were

combined as follows. Lymphocytes: “B cells naive”, “B cells memory”, “T cells CD4 naive”, “T cells CD4 memory resting”, “T cells CD4 memory activated”, “T cells follicular helper”, “T cells regulatory Tregs”, “T cells gamma delta”, “T cells CD8”, “NK cells resting”, “NK cells activated”, “Plasma cells”; CD4 T cells: “T cells CD4 naive”, “T cells CD4 memory resting”, “T cells CD4 memory activated”.

In vivo tumor growth studies

All animal experiments were performed in accordance with the Institutional Animal Care and Use Committee at Memorial Sloan Kettering Cancer Center (MSKCC). For the breast cancer model, female 6–8-week-old BALB/c or NSG mice (Jackson Laboratories) under isoflurane anesthesia were injected with cells in 100 µL of 50% Matrigel (Growth Factor Reduced, Corning) in phosphate-buffered saline (PBS). Cells were either 4T1 WT or *Atm*^{−/−} cells (3×10^5) injected into the inguinal mammary fat pad. For the colorectal cancer model, CT26 cells (5×10^5) WT or *Atm*^{−/−} were injected subcutaneously into the posterior flank. Mice with clinically palpable tumors (4 mm in diameter) were randomized into indicated treatment arms. RP-3500 or vehicle by oral gavage on a 3 days-on/4 days-off schedule at a previously established MTD³⁰ of 30 mg/kg. RP-3500 was administered in 0.5% methylcellulose/0.02% SDS vehicle. Etoposide was administered at 50 mg/kg single dose by intraperitoneal injection. IgG (2A3, Bio X Cell, 100 µg) or anti-PD-1 (RMP1-14, Bio X Cell 100 µg) antibodies were administered intraperitoneally in 100 µL of PBS twice weekly (every 3–4 days). For CD8⁺ T-cell depletion, anti-mouse CD8a antibody (2.43, Bio X Cell, 250 µg) was injected intraperitoneally at days 0, 3, 10 and 17 after the injection of 4T1 cells to the mammary fat pad. Mice were monitored by recording the body weights bi-weekly and tumor volumes were measured using calipers and calculated by the formula $(\text{length}) \times (\text{width})^2 / 2$. At the endpoint of the experiments, the mice were sacrificed to harvest the tumors and processed according to the assays. For IHC analysis, tumors were fixed in 10% buffered formalin, sectioned, and stained with CD3 antibody.

Microscopy

For immunofluorescence analyses, 1×10^4 cells were seeded in 4-well tissue culture slides (Lab-Tek II). After 18 hours, cells were irradiated at 10 Gy and 24 hours later cells were fixed in fixing solution (2% wt/vol paraformaldehyde, 0.1% Triton X-100 in PBS) for 10 min at room temperature, followed by permeabilization for 10 min in 0.5% vol/vol Triton X-100 in PBS. Fixed cells were blocked with blocking solution (10% vol/vol bovine calf serum in PBS) for 1 hour at room temperature and then incubated with γ-H2AX primary antibody (1:5,000 dilution in blocking solution; JWB301, Millipore) overnight at 4°C, washed three times with PBS and then incubated with Alexa Fluor 680-conjugated anti-mouse secondary antibodies (1:500 dilution in blocking solution; Invitrogen) for 1 hour. Cells

were then washed three times with PBS, counterstained, mounted in Vectashield Plus 6-diamidino-2-phenylindole dihydrochloride (Vector Laboratories), and visualized using a Nikon Ti2. At least 300 cells were counted for each sample. Cells with >5 foci were scored as γ -H2AX positive. The experiment was repeated at least three times.

Flow cytometry

Mice were sacrificed on day 16 after injecting the tumor cells and tumors were subsequently harvested. For the evaluation of CD8⁺ T-cell depletion, mice were sacrificed 21 days post-injection of the 4T1 cells and the spleen was dissected to isolate splenic lymphocytes. Tumor cells were dissociated with the Tumor Dissociation Kit (mouse; Miltenyi Biotec) with a gentleMACS Dissociator (Miltenyi Biotec) into suspension. Tumor cells then underwent processing in the following order: viability staining (Aqua L/D, Tonbo Biosciences), cell surface marker staining, fixation and permeabilization (Foxp3/Transcription Factor Staining Buffer Kit, Tonbo Biosciences), and intracellular staining. Data was acquired on a Cytex Aurora flow cytometer and analyzed using FlowJo software (TreeStar). Antibodies obtained from BD Biosciences: CD45 (30-F11) BUV395, CD4 (RM4-5) BUV496, CD8 (53-6.7) BV650, Ki-67 (B56) BV605, and PD-1 (RMP1-30) BB515. Antibodies obtained from BioLegend: TCR β (H57-597) PE and B220 (RA3-6B2) AF700. Antibodies obtained from Invitrogen: GzmB (GB11) APC.

Immunohistochemistry

Mouse tumors were fixed in 10% buffered formalin overnight at room temperature. The fixed tumors were processed and embedded in paraffin. IHC staining was performed by the Molecular Cytology Core Facility at MSKCC using CD3-Alexa 647. Tumor samples from patients with breast cancer with ATM biallelic mutations were stained with CD3, CD4 and CD8 antibodies performed on Ventana (Discovery XT platform) by the Laboratory of Comparative Pathology at MSKCC.

RNA sequencing

Tumor biopsy samples were collected from 35 patients out of which 58 samples (pre and on-Tx) could be used for RNA sequencing. RNA sequencing reads were aligned to the GRCh37 human genome using the STAR RNA sequencing aligner,⁵⁰ and then reads from transcripts were counted using the Genomic Alignments package in Bioconductor.^{51–52} Raw counts were transformed into Reads Per Kilobase per Million (RPKM) values by normalizing to sequencing depth and length of genes. Immune cell composition was predicted using CIBERSORTx in the absolute mode with batch corrected to minimize the impact of cross-platform variation.⁵³ Cell types of macrophages and T cells were combined for the further analysis. Macrophages: “M0”, “M1”, and “M2”; T cells: “T cells CD4 memory activated”, “T cells CD4 memory resting”, “T cells CD4 naïve”, “T cells CD8”, “T cells follicular helper”, “T cells gamma delta”, and “T cells regulatory (Tregs)”. The

cytolytic activity (CYT) score for each case was calculated according to the geometric mean of GZMA and PRF1 gene RPKM values. Mann-Whitney U test was used for cell fraction and CYT score comparisons.

Immunoblotting

Cells were irradiated at a dose of 10 Gy and after 4 hours non-irradiated and irradiated cells were lysed in an radio-immunoprecipitation assay buffer (RIPA) buffer with protease and phosphatase inhibitors (Thermo Fisher Scientific). Lysates were separated by SDS-PAGE (Bio-Rad, #5678085); then transferred to polyvinylidene fluoride membranes. Membranes were incubated with primary antibodies: anti-pKAP1 (S824; Abcam; ab133440), anti-KAP1 (Abcam; catalog no.10484), anti-ATM (Abcam; ab201022) and B-actin (Sigma; MAB1501R). Signal detection was carried out with secondary anti-rabbit (Jackson Immuno Research, #711-035-152) or anti-mouse (Jackson Immuno Research, #115-035-174) horseradish peroxidase antibody and SuperSignal West Dura Extended Duration Substrate (Thermo Fisher Scientific) using a Bio-Rad ChemiDoc Touch Imaging System (Bio-Rad).

Reverse transcription and quantitative real-time PCR

Total RNA was extracted from cells or tissues using RNeasy Plus Mini Kit (Qiagen). Reverse transcription was performed with SuperScript IV VILO Master Mix (Thermo Fisher Scientific). Quantitative PCR was performed with SYBR green master mix (Thermo Fisher Scientific) in duplicates using the gene-specific primers on the QuantStudio 6 Pro Real-Time PCR System (Applied Biosystems). Data were normalized against β -Actin. Primers for qRT-PCR are listed in online supplemental table 1.

Statistical analysis

Data were analyzed using GraphPad Prism. When comparing two groups for cell viability, messenger RNA expression, total blood count and tumor volume changes, statistical significance was calculated using unpaired two-tailed Student's t-tests. Two-way analysis of variance was used when comparing three or more groups for tumor growth. The statistical tests used are indicated in the figure legends. All statistical analyses were generated using GraphPad Prism V.9 software. Data were presented as mean \pm SD or mean \pm SEM with $p < 0.05$ considered statistically significant. Statistical significance was denoted as * $p < 0.05$; ** $p < 0.01$; *** $p < 0.001$; **** $p < 0.0001$. The number of independent experiments, samples or events was indicated in the figure legends. No data were excluded from the analyses. No statistical method was used to predetermine sample size. For all the in vivo experiments, animals were randomly assigned to experimental groups. The tumor size by volume in the treatment and control groups was similar before drug treatments.

Study approvals

Murine studies were conducted on protocol #21-02-002 and approved by the MSKCC Institutional Animal Care

and Use Committee (IACUC). Translational analysis from human specimens was approved on MSKCC IRB 22–222.

Author affiliations

¹Department of Radiation Oncology, Memorial Sloan Kettering Cancer Center, New York, New York, USA

²Department of Pathology, Memorial Sloan Kettering Cancer Center, New York, New York, USA

³Department of Pathology, Columbia University, New York, New York, USA

⁴Cancer Signaling and Microenvironment Program, Fox Chase Cancer Center, Philadelphia, PA, USA

⁵Memorial Sloan Kettering Cancer Center, New York, New York, USA

⁶Repare Therapeutics, Saint-Laurent, Quebec, Canada

⁷Repare Therapeutics, Boston, Massachusetts, USA

⁸MSKCC, New York, New York, USA

Present affiliations The present affiliation of Jorge Reis-Filho is: AstraZeneca, Gaithersburg, Maryland, USA.

X Xin Pei @isaacpei

Contributors Study Design and Conception: NR, JR-F, AK, MK. Murine Experiments: SS, VN. In vitro Experiments: AN, SS, JM, FD. Pathologic Analysis: FD, FP, JR-F. Genomic Data Analysis: YZ, SY, XP, ES, KM. Flow cytometric experiments: ALFL, RG, VN, MB-V. Interpretation of Data and Results: SS, NR, AR, SM, SP, LG, AK. Manuscript Writing: SS, JR-F, AK, NR, LG. Manuscript Approval: All authors. NR and SS take full responsibility for the veracity of all data and are guarantors for this manuscript.

Funding NR is supported by the STARR Cancer Consortium (#116-0064), NCI P50 CA257881-01, NCI P50 CA247749-01, and National Institutes of Health/ National Cancer Institute Cancer Center Support Grant P30 CA00874 and Repare Therapeutics. LG is/has been supported (as a PI unless otherwise indicated) by one R01 grant from the NIH/NCI (#CA271915), by two Breakthrough Level 2 grants from the US DoD BCRP (#BC180476P1, #BC210945), by a grant from the STARR Cancer Consortium (#116-0064), by a Transformative Breast Cancer Consortium Grant from the US DoD BCRP (#W81XWH2120034, PI: Formenti), by a U54 grant from NIH/NCI (#CA274291, PI: Deasy, Formenti, Weichselbaum), by the 2019 Laura Ziskin Prize in Translational Research (#ZP-6177, PI: Formenti) from the Stand Up to Cancer (SU2C), by a Mantle Cell Lymphoma Research Initiative (MCL-RI, PI: Chen-Kiang) grant from the Leukemia and Lymphoma Society (LLS), by a Rapid Response Grant from the Functional Genomics Initiative (New York, US), by a pre-SPORE grant (PI: Demaria, Formenti) and a Clinical Trials Innovation Grant from the Sandra and Edward Meyer Cancer Center (New York, US); by startup funds from the Dept. of Radiation Oncology at Weill Cornell Medicine (New York, US), by industrial collaborations with Lytix Biopharma (Oslo, Norway), Promontory (New York, US) and Onxeo (Paris, France), as well as by donations from Promontory (New York, US), the Luke Heller TECPR2 Foundation (Boston, US), Sotio a.s. (Prague, Czech Republic), Lytix Biopharma (Oslo, Norway), Onxeo (Paris, France), Ricerchiamo (Brescia, Italy), and Noxopharm (Chatswood, Australia). Funders did not have any role in design, collection, interpretation of the data, or writing of the report. Repare Therapeutics did provide consent to submit the manuscript for publication.

Competing interests NR receives research support from BMS, Pfizer, Repare Therapeutics, and Invitae. LG is/has been holding research contracts with Lytix Biopharma, Promontory and Onxeo, has received consulting/advisory honoraria from Boehringer Ingelheim, AstraZeneca, OmniSEQ, Onxeo, The Longevity Labs, Inzen, Invax, Sotio, Promontory, Noxopharm, EduCom, and the Luke Heller TECPR2 Foundation, and holds Promontory stock option.

Patient consent for publication Not applicable.

Ethics approval This study involves human participants and was approved by Memorial Sloan Kettering Cancer Center IRB 22–222. Participants gave informed consent to participate in the study before taking part.

Provenance and peer review Not commissioned; externally peer reviewed.

Data availability statement No data are available. This is a pre-clinical manuscript.

Supplemental material This content has been supplied by the author(s). It has not been vetted by BMJ Publishing Group Limited (BMJ) and may not have been peer-reviewed. Any opinions or recommendations discussed are solely those of the author(s) and are not endorsed by BMJ. BMJ disclaims all liability and responsibility arising from any reliance placed on the content. Where the content includes any translated material, BMJ does not warrant the accuracy and reliability

of the translations (including but not limited to local regulations, clinical guidelines, terminology, drug names and drug dosages), and is not responsible for any error and/or omissions arising from translation and adaptation or otherwise.

Open access This is an open access article distributed in accordance with the Creative Commons Attribution Non Commercial (CC BY-NC 4.0) license, which permits others to distribute, remix, adapt, build upon this work non-commercially, and license their derivative works on different terms, provided the original work is properly cited, appropriate credit is given, any changes made indicated, and the use is non-commercial. See <http://creativecommons.org/licenses/by-nc/4.0/>.

ORCID iD

Nadeem Riaz <http://orcid.org/0000-0001-9873-5862>

REFERENCES

- Pearl LH, Schierz AC, Ward SE, *et al.* Therapeutic opportunities within the DNA damage response. *Nat Rev Cancer* 2015;15:166–80.
- Roos WP, Thomas AD, Kaina B. DNA damage and the balance between survival and death in cancer biology. *Nat Rev Cancer* 2016;16:20–33.
- Hanahan D, Weinberg RA. Hallmarks of cancer: the next generation. *Cell* 2011;144:646–74.
- Groelly FJ, Fawkes M, Dagg RA, *et al.* Targeting DNA damage response pathways in cancer. *Nat Rev Cancer* 2023;23:78–94.
- Mouw KW, Goldberg MS, Konstantinopoulos PA, *et al.* DNA Damage and Repair Biomarkers of Immunotherapy Response. *Cancer Discov* 2017;7:675–93.
- Ma J, Setton J, Lee NY, *et al.* The therapeutic significance of mutational signatures from DNA repair deficiency in cancer. *Nat Commun* 2018;9:3292.
- Klapp V, Álvarez-Abrial B, Leuzzi G, *et al.* The DNA Damage Response and Inflammation in Cancer. *Cancer Discov* 2023;13:1521–45.
- Samstein RM, Lee C-H, Shoushtari AN, *et al.* Tumor mutational load predicts survival after immunotherapy across multiple cancer types. *Nat Genet* 2019;51:202–6.
- Cercek A, Lumish M, Sinopoli J, *et al.* PD-1 Blockade in Mismatch Repair–Deficient, Locally Advanced Rectal Cancer. *N Engl J Med* 2022;386:2363–76.
- Samstein RM, Krishna C, Ma X, *et al.* Mutations in *BRCA1* and *BRCA2* differentially affect the tumor microenvironment and response to checkpoint blockade immunotherapy. *Nat Cancer* 2021;1:1188–203.
- Vanpouille-Box C, Hoffmann JA, Galluzzi L. Pharmacological modulation of nucleic acid sensors - therapeutic potential and persisting obstacles. *Nat Rev Drug Discov* 2019;18:845–67.
- Marchi S, Guilbaud E, Tait SWG, *et al.* Mitochondrial control of inflammation. *Nat Rev Immunol* 2023;23:159–73.
- Parkes EE, Walker SM, Taggart LE, *et al.* Activation of STING-Dependent Innate Immune Signaling By S-Phase-Specific DNA Damage in Breast Cancer. *J Natl Cancer Inst* 2017;109:djw199.
- Pitter KL, Casey DL, Lu YC, *et al.* Pathogenic ATM Mutations in Cancer and a Genetic Basis for Radiotherapeutic Efficacy. *J Natl Cancer Inst* 2021;113:266–73.
- Derheimer FA, Kastan MB. Multiple roles of ATM in monitoring and maintaining DNA integrity. *FEBS Lett* 2010;584:3675–81.
- Lee JH, Paull TT. Cellular functions of the protein kinase ATM and their relevance to human disease. *Nat Rev Mol Cell Biol* 2021;22:796–814.
- Taylor AM, Harnden DG, Arlett CF, *et al.* Ataxia telangiectasia: a human mutation with abnormal radiation sensitivity. *Nature New Biol* 1975;258:427–9.
- Hu C, Hart SN, Gnanaolivu R, *et al.* A Population-Based Study of Genes Previously Implicated in Breast Cancer. *N Engl J Med* 2021;384:440–51.
- Cancer Genome Atlas Research Network. Comprehensive molecular profiling of lung adenocarcinoma. *Nature New Biol* 2014;511:543–50.
- Mandal R, Samstein RM, Lee K-W, *et al.* Genetic diversity of tumors with mismatch repair deficiency influences anti-PD-1 immunotherapy response. *Science* 2019;364:485–91.
- Ma X, Riaz N, Samstein RM, *et al.* Functional landscapes of POLE and POLD1 mutations in checkpoint blockade-dependent antitumor immunity. *Nat Genet* 2022;54:996–1012.
- Shiloh Y, Ziv Y. The ATM protein kinase: regulating the cellular response to genotoxic stress, and more. *Nat Rev Mol Cell Biol* 2013;14:197–210.
- Barlow C, Hirotsune S, Paylor R, *et al.* Atm-deficient mice: a paradigm of ataxia telangiectasia. *Cell* 1996;86:159–71.

- 24 Kim J, Wong PKY. Loss of ATM impairs proliferation of neural stem cells through oxidative stress-mediated p38 MAPK signaling. *Stem Cells* 2009;27:1987–98.
- 25 Haj M, Frey Y, Levon A, et al. The cGAS-STING, p38 MAPK, and p53 pathways link genome instability to accelerated cellular senescence in ATM-deficient murine lung fibroblasts. *Proc Natl Acad Sci U S A* 2025;122:e2419196122.
- 26 Zhu Y, Pei X, Novaj A, et al. Large-scale copy number alterations are enriched for synthetic viability in BRCA1/BRCA2 tumors. *Genome Med* 2024;16:108.
- 27 Le DT, Durham JN, Smith KN, et al. Mismatch repair deficiency predicts response of solid tumors to PD-1 blockade. *Science* 2017;357:409–13.
- 28 Pantelidou C, Sonzogno O, De Oliveria Taveira M, et al. PARP Inhibitor Efficacy Depends on CD8⁺ T-cell Recruitment via Intratumoral STING Pathway Activation in BRCA-Deficient Models of Triple-Negative Breast Cancer. *Cancer Discov* 2019;9:722–37.
- 29 Ding L, Kim H-J, Wang Q, et al. PARP Inhibition Elicits STING-Dependent Antitumor Immunity in Brca1-Deficient Ovarian Cancer. *Cell Rep* 2018;25:2972–80.
- 30 Ngoi NYL, Peng G, Yap TA. A Tale of Two Checkpoints: ATR Inhibition and PD-(L)1 Blockade. *Annu Rev Med* 2022;73:231–50.
- 31 Sugitani N, Vendetti FP, Cipriano AJ, et al. Thymidine rescues ATR kinase inhibitor-induced deoxyuridine contamination in genomic DNA, cell death, and interferon- α/β expression. *Cell Rep* 2022;40:111371.
- 32 Williams KM, Hakim FT, Gress RE. T cell immune reconstitution following lymphodepletion. *Semin Immunol* 2007;19:318–30.
- 33 Kornepati AVR, Rogers CM, Sung P, et al. The complementarity of DDR, nucleic acids and anti-tumour immunity. *Nature New Biol* 2023;619:475–86.
- 34 Härtlova A, Erttmann SF, Raffi FA, et al. DNA damage primes the type I interferon system via the cytosolic DNA sensor STING to promote anti-microbial innate immunity. *Immunity* 2015;42:332–43.
- 35 Weigelt B, Bi R, Kumar R, et al. The Landscape of Somatic Genetic Alterations in Breast Cancers From ATM Germline Mutation Carriers. *J Natl Cancer Inst* 2018;110:1030–4.
- 36 Zitvogel L, Galluzzi L, Kepp O, et al. Type I interferons in anticancer immunity. *Nat Rev Immunol* 2015;15:405–14.
- 37 Boukhaled GM, Harding S, Brooks DG. Opposing Roles of Type I Interferons in Cancer Immunity. *Annu Rev Pathol* 2021;16:167–98.
- 38 Dunphy G, Flannery SM, Almine JF, et al. Non-canonical Activation of the DNA Sensing Adaptor STING by ATM and IFI16 Mediates NF- κ B Signaling after Nuclear DNA Damage. *Mol Cell* 2018;71:745–60.
- 39 Galluzzi L, Guilbaud E, Schmidt D, et al. Targeting immunogenic cell stress and death for cancer therapy. *Nat Rev Drug Discov* 2024;23:445–60.
- 40 Kroemer G, Galassi C, Zitvogel L, et al. Immunogenic cell stress and death. *Nat Immunol* 2022;23:487–500.
- 41 Dillon MT, Bergerhoff KF, Pedersen M, et al. ATR Inhibition Potentiates the Radiation-induced Inflammatory Tumor Microenvironment. *Clin Cancer Res* 2019;25:3392–403.
- 42 Zhang Q, Green MD, Lang X, et al. Inhibition of ATM Increases Interferon Signaling and Sensitizes Pancreatic Cancer to Immune Checkpoint Blockade Therapy. *Cancer Res* 2019;79:3940–51.
- 43 Baklaushev VP, Kilpeläinen A, Petkov S, et al. Luciferase Expression Allows Bioluminescence Imaging But Imposes Limitations on the Orthotopic Mouse (4T1) Model of Breast Cancer. *Sci Rep* 2017;7:7715.
- 44 Hu M, Zhou M, Bao X, et al. ATM inhibition enhances cancer immunotherapy by promoting mtDNA leakage and cGAS-STING activation. *J Clin Invest* 2021;131:e139333.
- 45 Mehta A, Merkel OM. Immunogenicity of Cas9 Protein. *J Pharm Sci* 2020;109:62–7.
- 46 Roulston A, Zimmermann M, Papp R, et al. RP-3500: A Novel, Potent, and Selective ATR Inhibitor that is Effective in Preclinical Models as a Monotherapy and in Combination with PARP Inhibitors. *Mol Cancer Ther* 2022;21:245–56.
- 47 Thorsson V, Gibbs DL, Brown SD, et al. The Immune Landscape of Cancer. *Immunity* 2018;48:812–30.
- 48 Riaz N, Blecua P, Lim RS, et al. Pan-cancer analysis of bi-allelic alterations in homologous recombination DNA repair genes. *Nat Commun* 2017;8:857.
- 49 Newman AM, Steen CB, Liu CL, et al. Determining cell type abundance and expression from bulk tissues with digital cytometry. *Nat Biotechnol* 2019;37:773–82.
- 50 Dobin A, Davis CA, Schlesinger F, et al. STAR: ultrafast universal RNA-seq aligner. *Bioinformatics* 2013;29:15–21.
- 51 Lawrence M, Huber W, Pagès H, et al. Software for computing and annotating genomic ranges. *PLoS Comput Biol* 2013;9:e1003118.
- 52 Gentleman RC, Carey VJ, Bates DM, et al. Bioconductor: open software development for computational biology and bioinformatics. *Genome Biol* 2004;5:R80.
- 53 Chen B, Khodadoust MS, Liu CL, et al. Profiling Tumor Infiltrating Immune Cells with CIBERSORT. *Methods Mol Biol* 2018;1711:243–59.